ISTITUTO NAZIONALE DI FISICA NUCLEARE

Sezione di Trieste

INFN/TC-94/09

16 maggio 1994

F. Arfelli, G. Barbiellini, G. Cantatore, E. Castelli, P. Cristaudo, L. Dalla Palma, M. Di Michiel, R. Longo, P. Poropat, R. Rosei, M. Sessa, F. Tomasini, G. Tromba, A.Vacchi

SILICON X-RAY DETECTOR FOR SYNCHROTRON RADIATION DIGITAL RADIOLOGY

Servizio Documentazione
dei Laboratori Nazionali di Frascati

Silicon X-ray detector for synchrotron radiation digital radiology

F. Arfelli, G. Barbiellini, G. Cantatore, E. Castelli, P. Cristaudo, M. Di Michiel, P. Poropat, R. Rosei, M. Sessa, F. Tomasini, A. Vacchi
Dipartimento di Fisica dell' Università di Trieste, Italy
and
Sezione INFN di Trieste, Italy

L. Dalla Palma, R. Longo,
Istituto di Radiologia dell' Università di Trieste, Italy
and
USL - Trieste, Italy

R. Rosei, G. Tromba,
Società Sincrotrone Trieste, Italy

Presented to the
"1994 SYMPOSIUM ON RADIATION MEASUREMENTS AND APPLICATIONS"
May 16-20, 1994, the University of Michigan

Abstract

The SYRMEP Collaboration (SYnchrotron Radiation for MEdical Physics), is conducting a research project in digital mammography and plans to use a monochromatic X-ray beam provided by Elettra, the synchrotron radiation facility in operation in Trieste (Italy), in conjunction with a novel silicon pixel detector.

A set of silicon strip detectors was arranged to form a matrix of pixels. This prototype with a sensitive area of 24 x 1 mm^2 (i.e. 2x48 pixels of 0.5 x 0.5 mm^2) has been used to produce images with X-rays.

Introduction

In this paper we present the development of a facility dedicated to the study of digital radiology for medical applications. The project progresses along two directions: the use of synchrotron radiation to obtain a monochromatic source of X-rays, and the construction of a high granularity, high efficiency, detector to produce digital images in real time [1, 2, 3]. This detector will provide, while requiring a lower radiation dose compared with current standards, complementary information to conventional radiology and open the way for new diagnostic tools.

The synchrotron beamline under construction at the Elettra facility in Trieste will provide, at a distance of about 20 m from an Elettra bending magnet, a monochromatic, laminar section (~150x4 mm^2), X-ray beam. This beam will illuminate the silicon pixel detector especially developed for this purpose. We present in the following the characteristics of such a detector, and the results obtained with a prototype.

The SYRMEP silicon detector

Silicon detectors have been usually built with thicknesses of the order of 1 mm. Structures are implanted on the large face of the silicon wafer, and in the usual applications radiation impinges on this same surface. In the geometry we are considering, the X-rays are impinging from the thin side of the detector (see Figure 5 in [4]) removing any practical limitation on the thickness of the absorbing silicon, therefore achieving the highest possible detection efficiency. In this configuration the geometry of the detector defines the granularity or the pixel size: one coordinate is given by the silicon slab thickness, and the other is determined by the pitch of the implanted strips. Each single detector element can in principle be positioned in a stack to enlarge the sensitive area. This approach will be best exploited when a high density integrated electronics, performing most of the required signal processing, will be available.

The main source of noise in silicon detectors is the junction reverse current. In the design stage, implanted strips are kept at some distance from the current generating region near the edge, where the crystal is cut. As a consequence, there is a dead area near the edge of the detector: X-rays absorbed in this region do not produce a signal. This is the only limitation to the efficiency of a detector used in this configuration. Usually the dead region has a depth of 200 to 500 μm of Si (in practice it is the

thickness of the detector). Efficiencies at three different X-ray energies for several depths of the dead region are given in Table 1a, while Table 1b gives the efficiencies at several energies as a function of detector depth for a 200 μm deep dead area. Stacking several detectors will also add a dead area due to bondings.

The prototype detector discussed in the present paper has a pixel size of 0.5x0.5 mm^2, and consists of two layers, each having 48 pixels. Each pixel has its own electronic chain for signal detection and read-out. To test the imaging capabilities of this device we placed a Cd 109 radioactive source in a fixed position with respect to the detector, while tests objects were moved by means of a micropositioning device between source and detector in order to scan the whole object volume. Spatial resolution could then be increased by scanning with a step smaller than pixel dimensions.

Read-out electronics

Figure 1 shows a block diagram of the read-out electronics relative to a single channel. The charge signal due to the passage of an X-ray within the active volume of one pixel is collected and amplified by a hybrid charge sensitive amplifier. Further amplification and shaping are provided by a shaping amplifier, the output of which, having an amplitude proportional to the energy deposited by the incoming radiation, is fed into a discriminator unit. The resulting logic signals are collected and counted by a CAMAC scaler (Mod. 4434, LeCroy Corp., Chestnut Ridge NY, U.S.A.). Scaler data are then read over the CAMAC bus by a Macintosh IIfx computer and stored for subsequent processing. The computer is also connected, via an IEEE488 bus, to a micropositioning drive control unit (Mod. ITL09, Micro Controle, Evry Cedex, France) which controls the scanning motion.

Preamplifier characteristics have been measured using calibrated input pulses with a fast risetime (~100 ns) and a long decay time constant (>50 μs). Figure 2 shows the preamplifier response to pulses injecting a given total charge. Peaks representing different input charges are positioned on the horizontal axis according to the corresponding output charge. The graphs in Figure 3 are obtained from these data. Figure 3a shows a plot of the output charge versus the input charge (or the equivalent energy deposit in Si). A least-squares fit to a straight line of the data gives a gain of $(48\pm1)x10^3$. Figure 3b shows a plot of preamplifier gain versus input charge. Figure 4 details the circuit used to implement the shaping and discrimination stages of the read-out. The charge amplifier output is fed into the J1 terminal. The IC chip labeled U1 is

the shaping amplifier, U2 is the discriminator, and U3 performs a logic translation from NIM to ECL standards. The J2 terminals are connected to the CAMAC scaler. This circuit has been mounted on a custom designed PC board.

To characterize the system response to radiation of given energy, we measured the spectrum of a Cd 109 radioactive point source. Figure 5 shows the Cd 109 spectrum obtained with the electronic chain just described. The relative depth of the valley between the pedestal and the 22 keV peak ensures that a meaningful energy threshold can be set by our discriminator. Energy resolution is found to be ±16%. Energy thresholds were checked to be fairly uniform over all the 96 detector channels. The measured maximum input pulse rate accepted by the readout chain is 40 kHz. Thus, up to this rate, our detector is able to perform single photon counting down to energies as low as 20 keV. The output capacitance limits the signal to noise performance of the system [5]. For low energy X-rays this is relevant, and can also result in reduced detection efficiency.

Imaging results

Various test objects, or phantoms, were used to test the imaging capabilities of the detector system described above. To detail the spatial resolution we were able to achieve, we used a pair of ~230 μm diameter copper wires joined at two points by soldering. The average separation of the two wires between the joints was ~100 μm. The sample was scanned with a 50 μm step. Figure 6 shows the results of this imaging run. False color raw data are shown on the left hand side, while on the right hand side processed data show the separation between the two wires. Image processing and reconstruction from raw data will be briefly discussed below. To obtain this image, a superficial dose, considering a laminar beam, of 52 μGy was delivered to the sample. Figure 7 shows the image obtained of a standard X-ray test pattern at 4.5 line-pairs/mm, corresponding to a spatial resolution of 110 μm. Figure 7a shows a profile plot of the test pattern while Figure 7b shows a false color image of the same test pattern. Superficial dose was 62 μGy. Finally we show in Figure 8 images of a detail from a standard mammography phantom. The detail is a 6 mm diameter, 75 μm thick, Al disk embedded in 16 mm thick plexiglas. The upper images show raw data and reconstructed data, on the left and on the right hand side respectively. The lower images are false color renditions of the same data. The scanning step was 250 μm, and the superficial dose was 131 μGy. Note that when adding 75 μm of Al to 16 mm of plexiglas absorption changes only by about 4%.

Image reconstruction

When processing raw data from an imaging system one must take into account the way the instrument will respond to a given signal. If we consider the "true" image of a test object to be represented by some function $I(\mathbf{x})$ of the spatial coordinates, and the raw data by a function $C(\mathbf{x})$ which can be expressed as a convolution product, then [6,7]

$$C(\mathbf{x}) = I(\mathbf{x}) \otimes H(\mathbf{x}) + n(\mathbf{x}), \tag{1}$$

where $H(\mathbf{x})$ is the instrument response to a Dirac delta, and $n(\mathbf{x})$ represent the noise. To reconstruct the true image, Equation 1 is Fourier-transformed and a filtering function $\tilde{R}(\mathbf{k})$ is applied so that

$$\tilde{I}_{rec}(\mathbf{k}) = \tilde{C}(\mathbf{k})\tilde{R}(\mathbf{k}) = \tilde{C}(\mathbf{k})\frac{\tilde{\Phi}(\mathbf{k})}{\tilde{H}(\mathbf{k})} = \tilde{\Phi}(\mathbf{k})\tilde{I}(\mathbf{k}) + \tilde{n}(\mathbf{k})\frac{\tilde{\Phi}(\mathbf{k})}{\tilde{H}(\mathbf{k})}. \tag{2}$$

A common criterion for the choice of the function $\tilde{\Phi}(\mathbf{k})$ requires that $\int |I(\mathbf{x}) - I_{rec}(\mathbf{x})|^2 d\mathbf{x}$ be minimum. In our case, to a good approximation

$$\tilde{\Phi}(\mathbf{k}) = \frac{\left|\tilde{H}(\mathbf{k})\right|^2}{\left|\tilde{H}(\mathbf{k})\right|^2 + W}, \tag{3}$$

where W is a constant chosen on the basis of the signal-to-noise ratio. Equation 3 contains quantities amenable to an experimental determination. In fact, $\tilde{H}(\mathbf{k})$ can be derived from the instrument response to a pointlike image. As a final step, an inverse Fourier-transformation of Equation 2 yields the reconstructed image.

Conclusions

The results discussed above clearly show that the detection and single photon counting of X-rays having energies of interest for the application to medical diagnostics are indeed possible using the SYRMEP silicon detector. From the imaging point of view, our detector can achieve a good contrast resolution, for instance when imaging a mammography phantom. Spatial resolution can also be increased by reducing the scanning step at the price of a higher radiation dose.

We foresee, as our next step, a detector with smaller pixels (0.2 x 0.3 mm^2), and about 500 channels, while our final objective is to build a detector with a sensitive area covering the entire beam section (~150 x 4 mm^2), in order to minimize the dose delivered to the phantom. This will constitute an obvious advantage for future applications to the actual diagnostic practice. Furthermore, the final detector assembly will require "ad hoc" VLSI read-out electronics, which must be developed for our special purposes.

As a final remark, we point out that a key characteristic of this project is the single-photon-counting capability of our detectors, which enables us to extract the maximum information from the X-ray beam while keeping the dose at a minimum level.

References

[1] F. Arfelli et al., SYnchrotron Radiation for MEdical Physics. A comparison between digital and conventional screen-film images, Phys. Med., Vol. IX (1993) p.175.

[2] A. Vacchi, Silicon radiation detectors developments in digital radiology for synchrotron radiation, Phys. Med., Vol. IX (1993) p. 155.

[3] F. Arfelli et al., SYRMEP(SYnchrotron Radiation for MEdical Physics). Performance of the digital detection system, Phys. Med., Vol. IX, Suppl. 1 (1993) p.229.

[4] L. Benini et al., Synchrotron radiation application to digital mammography. A proposal for the Trieste project "Elettra", Phys. Med., Vol. VI (1990) p.293.

[5] E. Gatti, P.F. Manfredi, Processing the signals from solid-state detectors in elementary particle physics, La Rivista del Nuovo Cimento, Vol. 9, no. 1 (1986).

[6] W. H. Pratt, Digital Image Processing, Wiley, New York (1978)

[7] J. S. Lim, Two Dimensional Signal and Image Processing, Prentice-Hall, Englewood Cliffs, New Jersey (1990).

Table 1a

Dead area thickness	Eff. @ 15 keV	Eff. @ 20 keV	Eff. @ 25 keV
100 μm	78 %	89 %	94 %
150 μm	69 %	85 %	91 %
200 μm	61 %	80 %	89 %
300 μm	47 %	72 %	84 %
400 μm	37 %	65 %	79 %
500 μm	28 %	58 %	75 %

Table 1b

	Detector absorption depth			
Energy	0.5 cm	0.75 cm	1.0 cm	2.5 cm
15 keV	61 %	61 %	61 %	61 %
20 keV	80 %	80 %	80 %	80 %
25 keV	83 %	88 %	89 %	89 %
30 keV	76 %	86 %	90 %	93 %
40 keV	54 %	69 %	78 %	95 %
50 keV	39 %	53 %	63 %	90 %

Table 1

Detector efficiencies for various X-ray energies taking into account both photoelectric and Compton processes.

a) Efficiencies at three different energies as a function of dead area depth. Detector absorption depth is 1 cm.

b) Efficiencies at several energies as a function of detector absorption depth. Dead area depth is 200 μm.

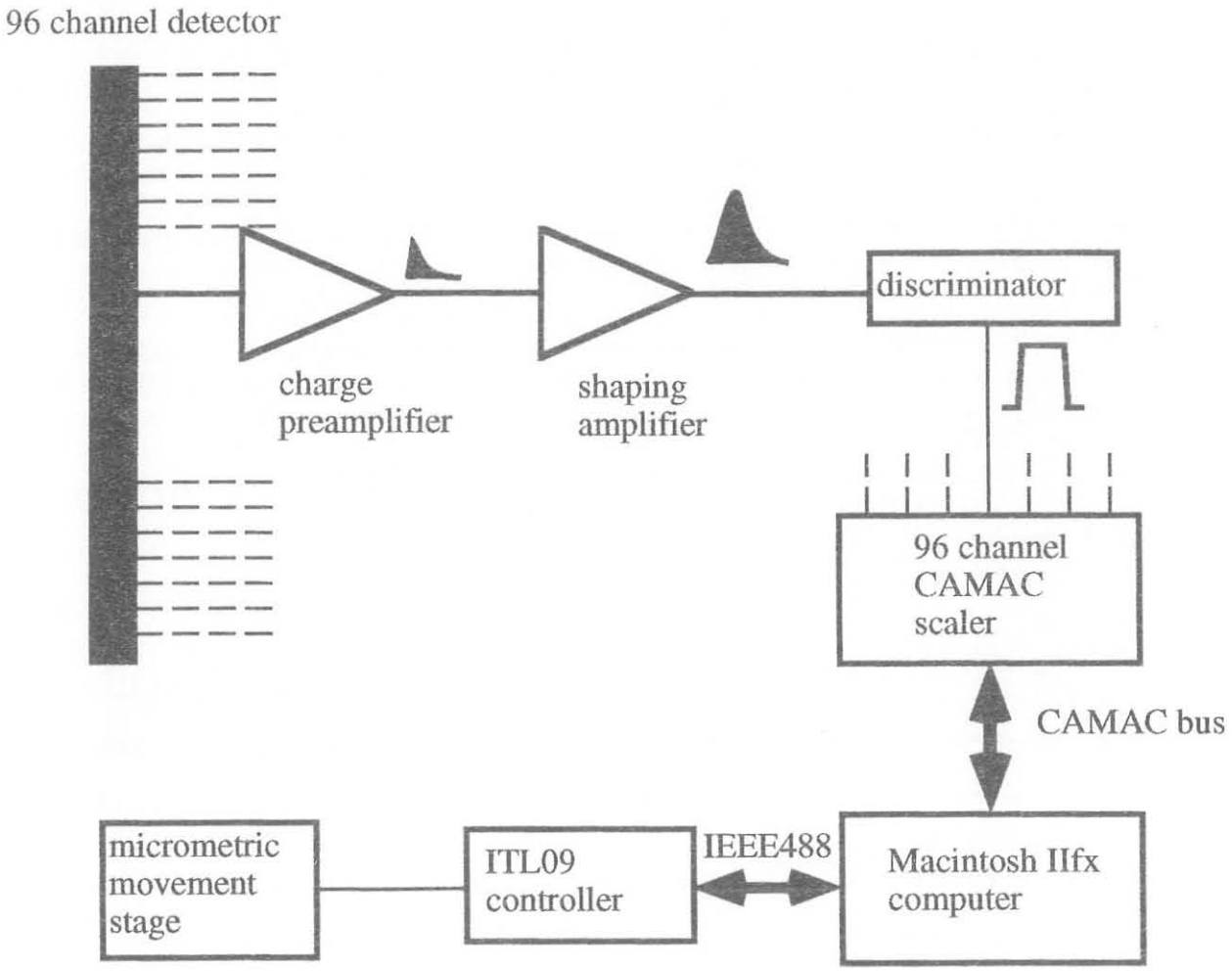

Figure 1 : Block diagram of the read-out electronics.

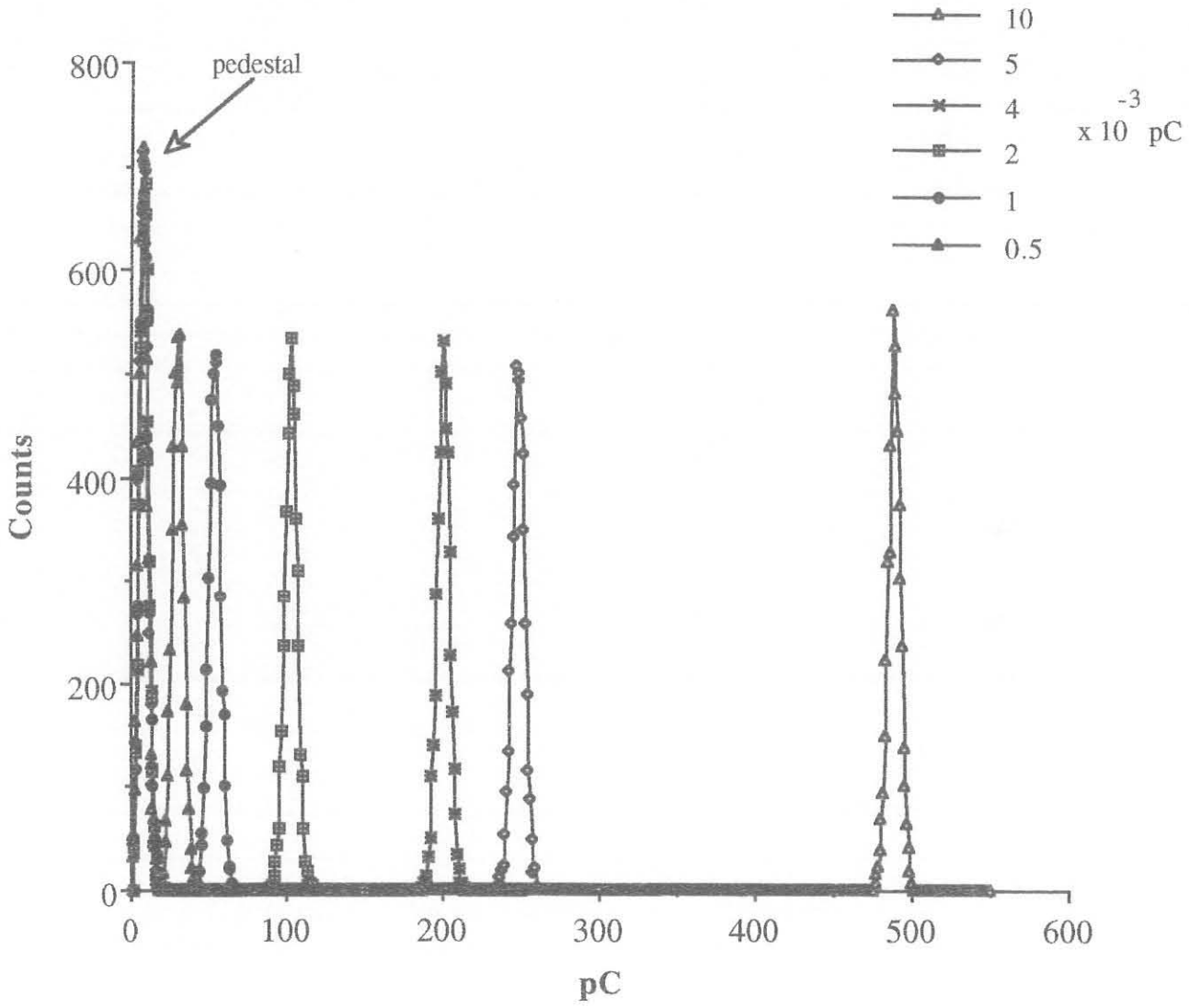

Figure 2 : Preamplifier response to a given input charge.

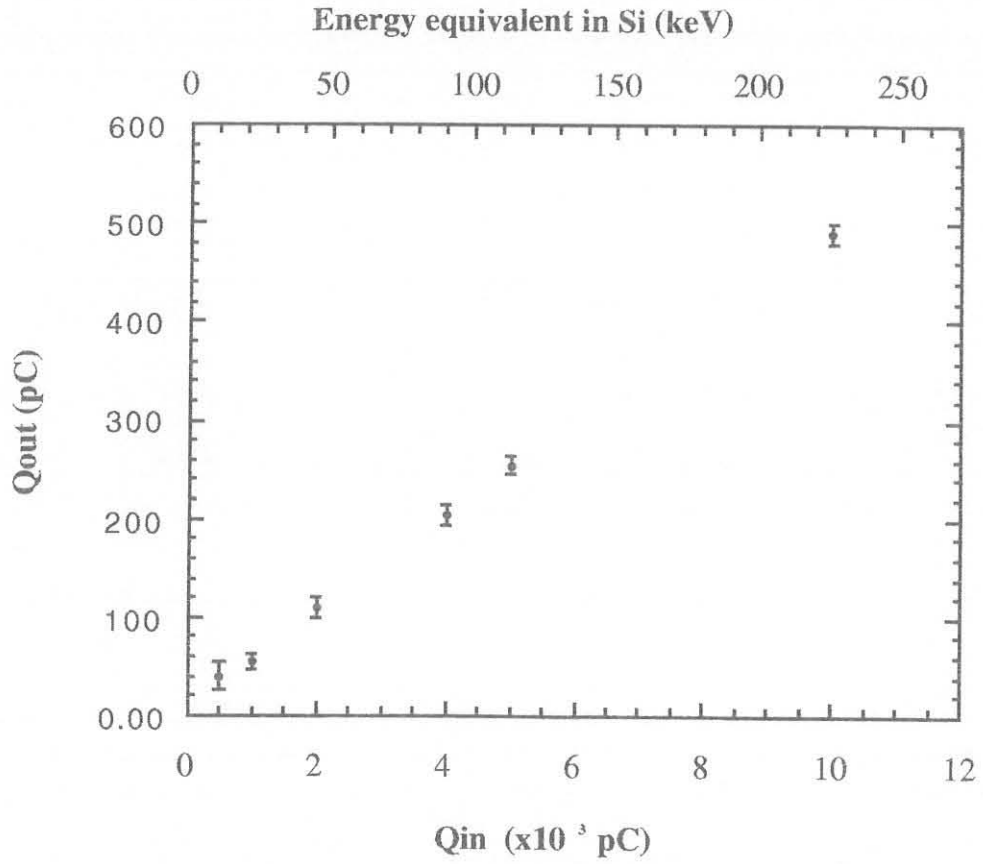

Figure 3 a : Preamplifier gain curves (see text). Output charge versus input charge.

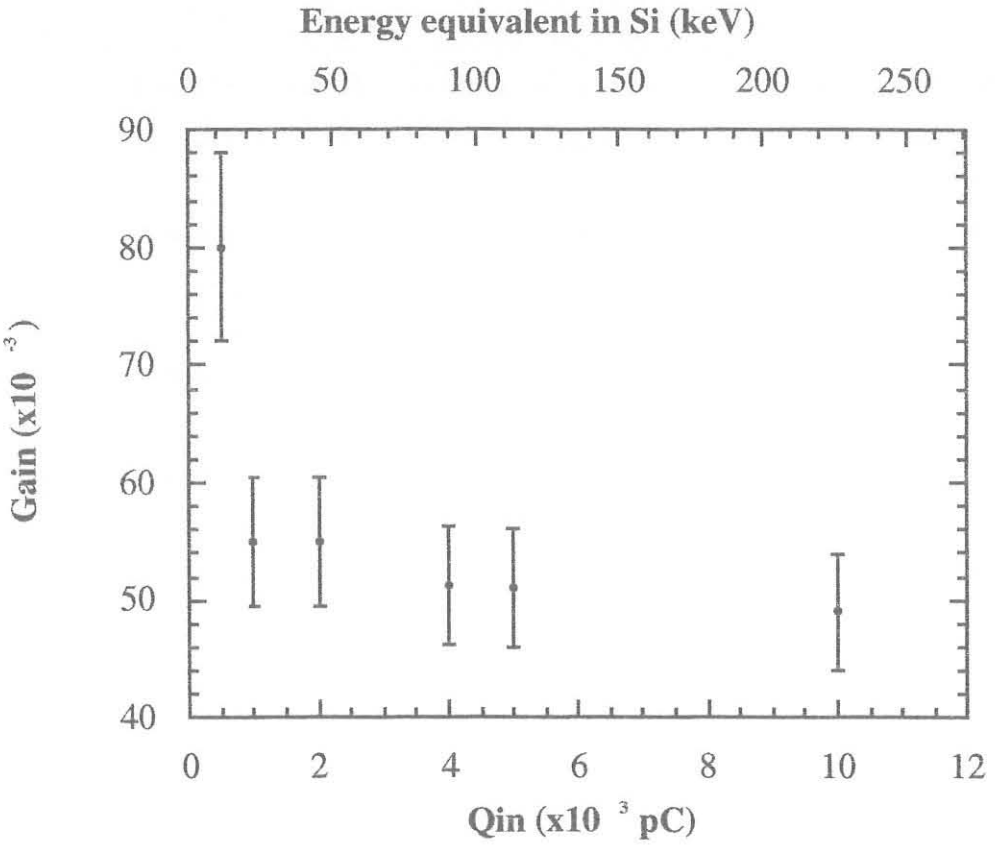

Figure 3 b : Preamplifier gain curves (see text).b) Gain versus input charge.

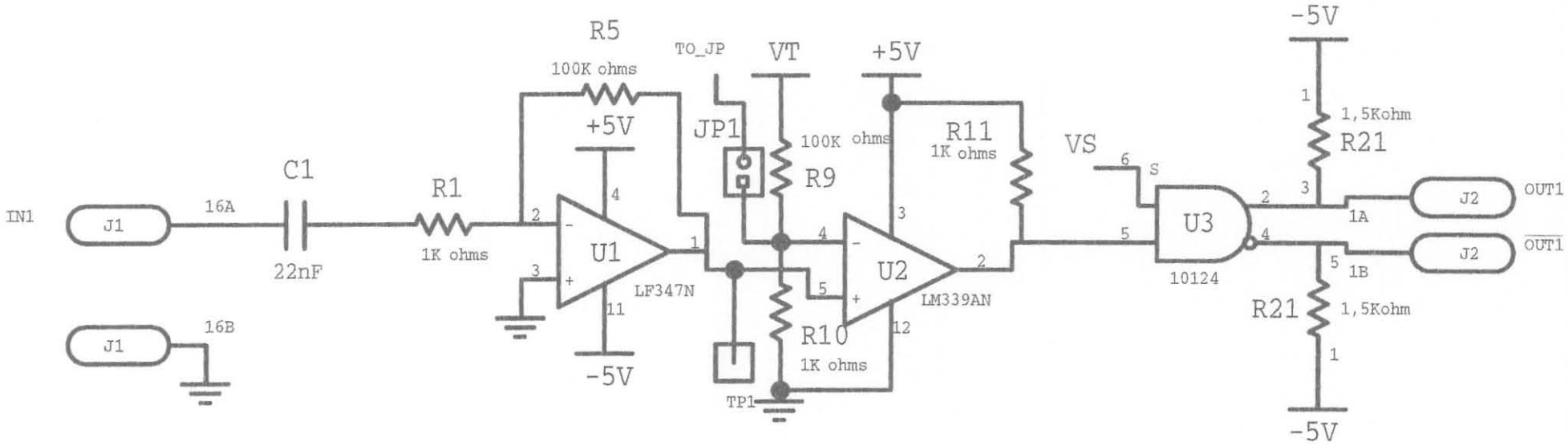

Figure 4 : Circuit schematic of a readout channel.

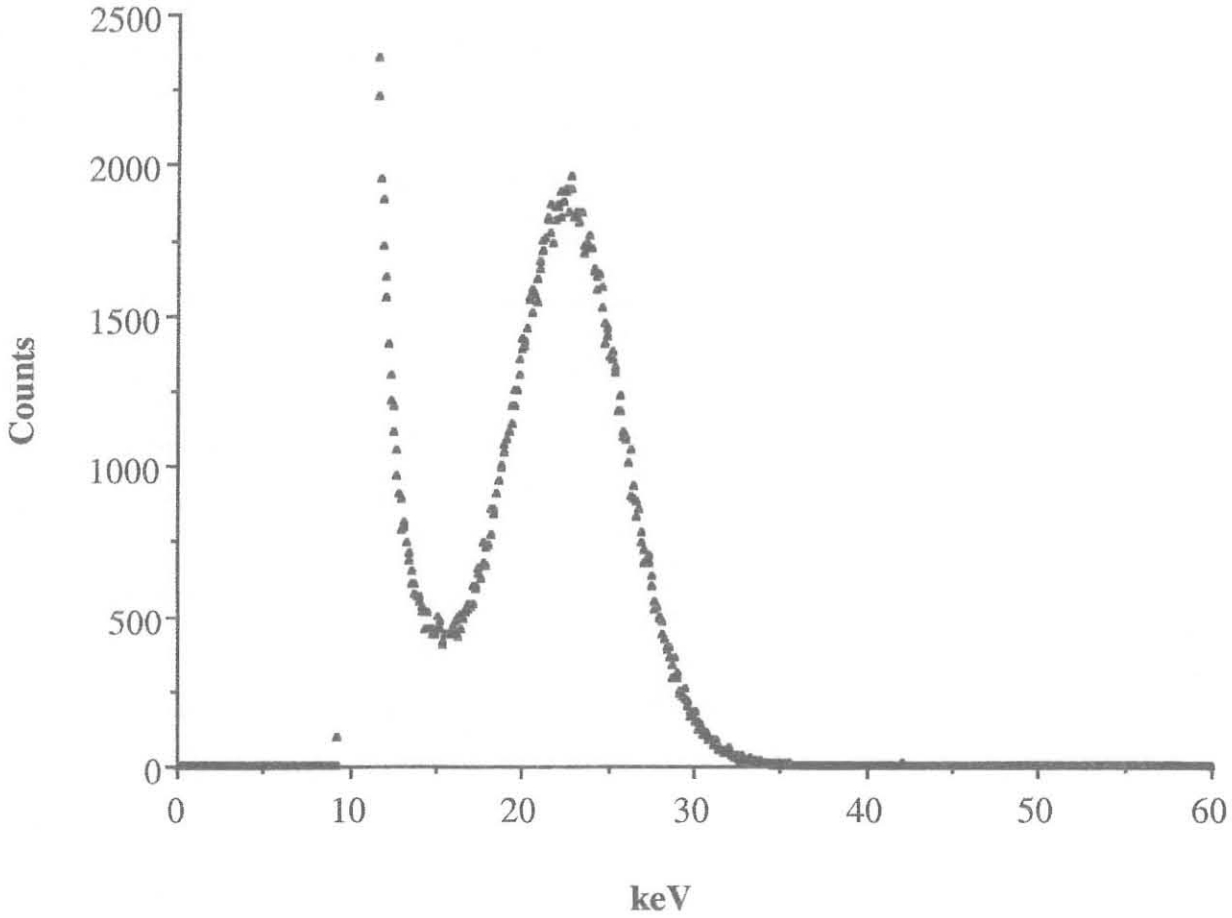

Figure 5 : Spectrum of a Cd 109 radioactive source.

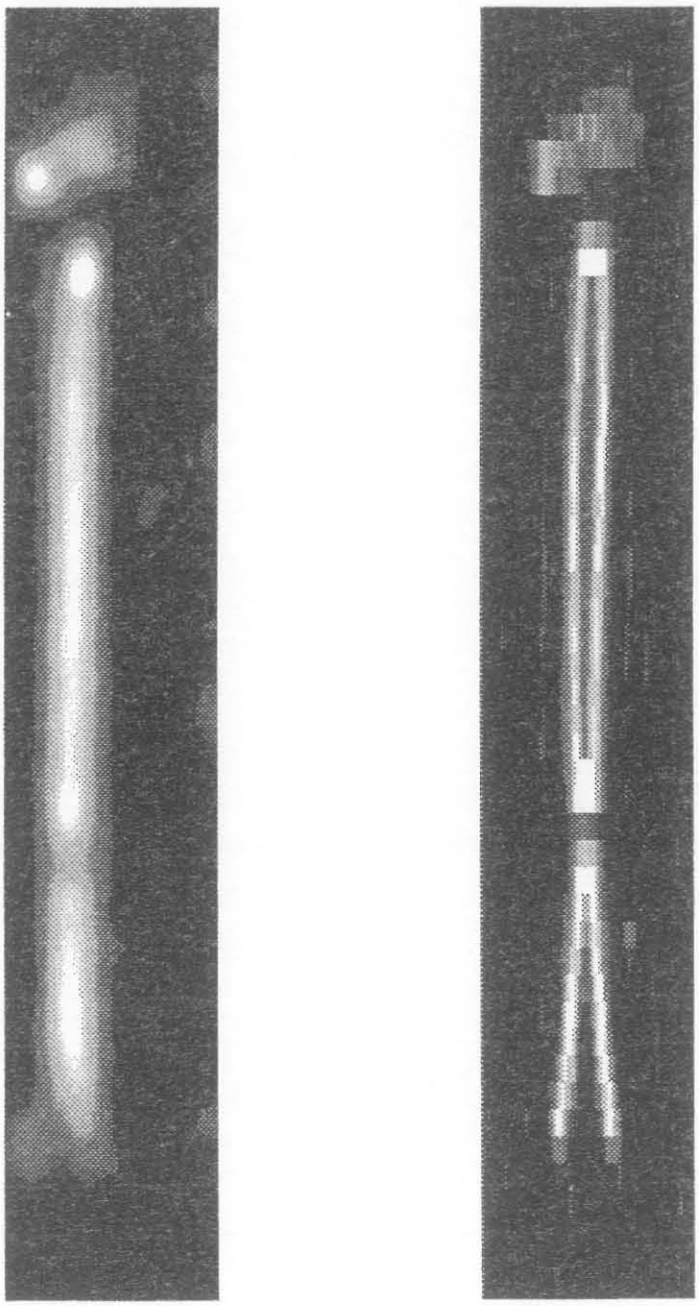

Figure 6 : Digital images of two copper wires (see text).

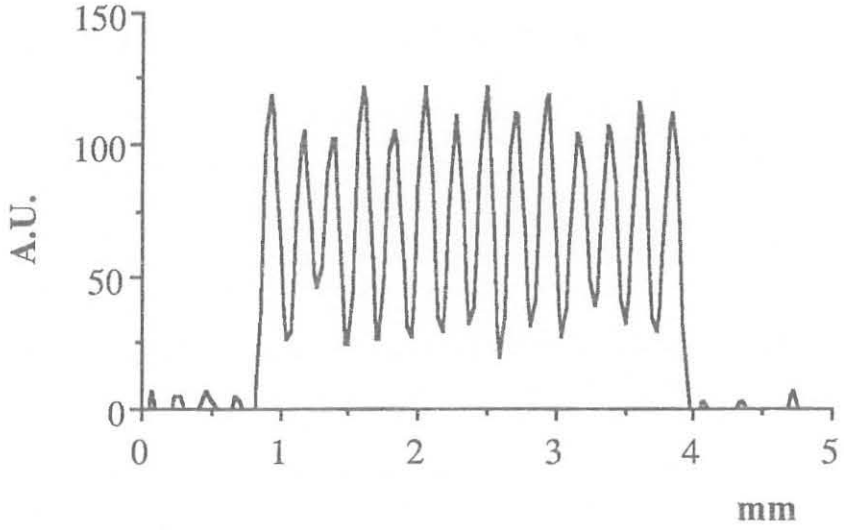

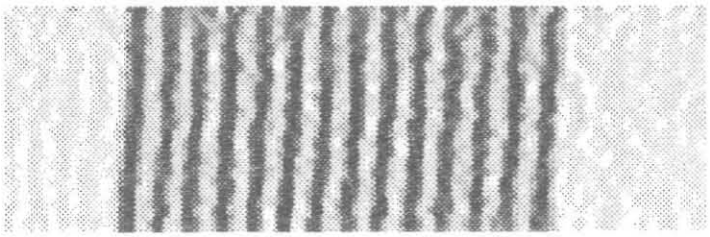

Figure 7 : Profile plot and digital image of a 4.5 line-pair/mm X-ray test pattern (see text).

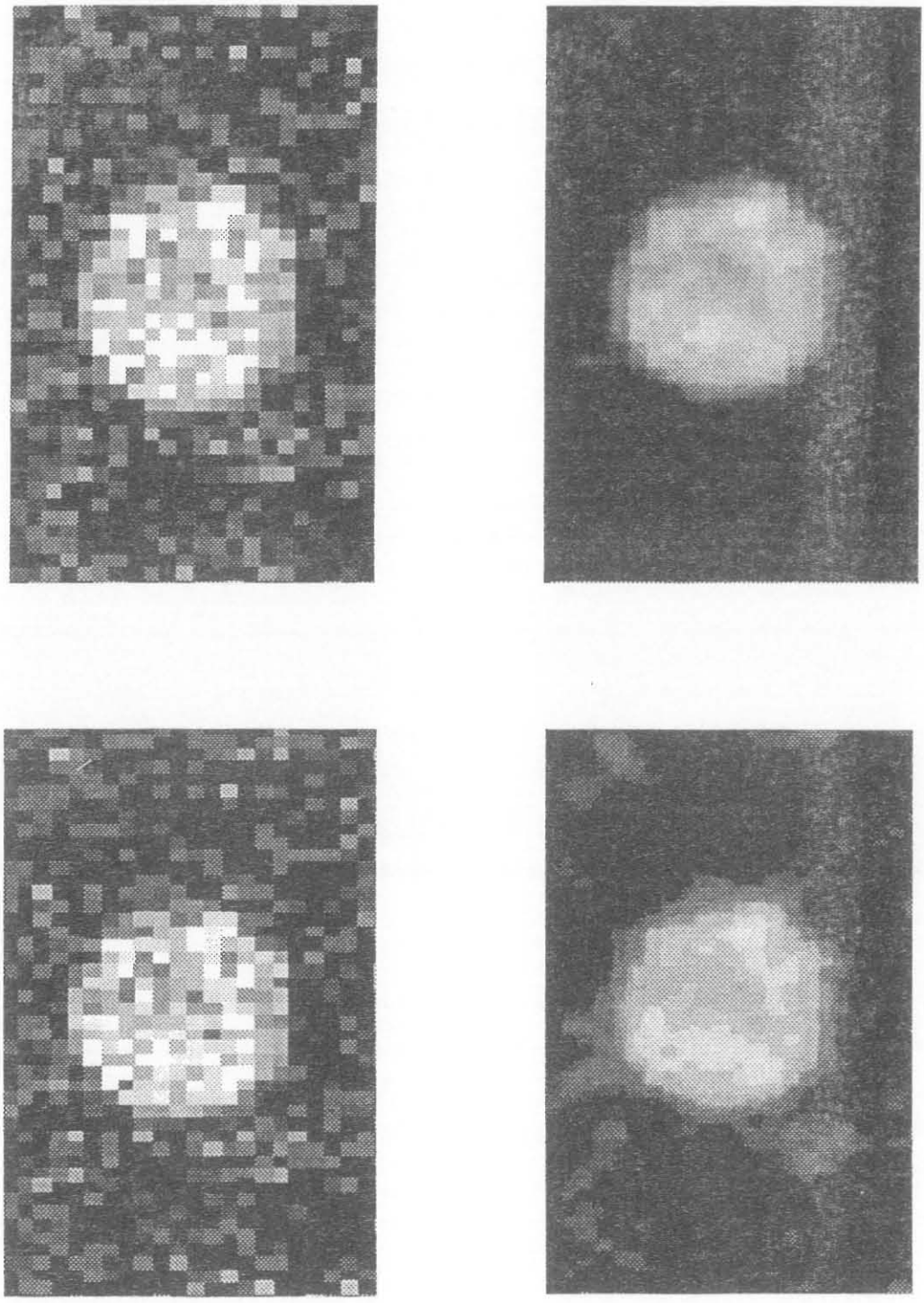

Figure 8 : Digital images of a detail of a standard mammographic phantom (see text).